PHYSICAL REVIEW D **87,** 036004 (2013)

Phase diagram and surface tension in the three-flavor Polyakov-quark-meson model

B. W. Mintz,[1,*] R. Stiele,[2,†] Rudnei O. Ramos,[1,‡] and J. Schaffner-Bielich[2,3,4,§]

[1]*Departamento de Física Teórica, Universidade do Estado do Rio de Janeiro, 20550-013 Rio de Janeiro, Rio de Janeiro, Brazil*
[2]*Institut für Theoretische Physik, Ruprecht-Karls-Universität Heidelberg, Philosophenweg 16, D-69120 Heidelberg, Germany*
[3]*Institut für Theoretische Physik, Goethe-Universität Frankfurt, Max-von-Laue-Straße 1, D-60438 Frankfurt am Main, Germany*
[4]*ExtreMe Matter Institute EMMI, GSI Helmholtzzentrum für Schwerionenforschung GmbH, Planckstraße 1, D-64291 Darmstadt, Germany*

(Received 11 December 2012; published 6 February 2013)

We obtain the in-medium effective potential of the three-flavor Polyakov-quark-meson model as a real function of real variables in the Polyakov loop variable, to allow for the study of all possible minima of the model. At finite quark chemical potential, the real and imaginary parts of the effective potential, in terms of the Polyakov loop variables, are made apparent, showing explicitly the fermion sign problem of the theory. The phase diagram and other equilibrium observables, obtained from the real part of the effective potential, are calculated in the mean-field approximation. The obtained results are compared to those found with the so-called saddle point approach. Our procedure also allows the calculation of the surface tension between the chirally broken and confined phase and the chirally restored and deconfined phase. The values of surface tension we find for low temperatures are very close to the ones recently found for two-flavor chiral models. Some consequences of our results for the early Universe, for heavy-ion collisions, and for proto-neutron stars are discussed.

DOI: 10.1103/PhysRevD.87.036004 PACS numbers: 25.75.Nq, 64.60.Q−, 11.30.Rd, 98.80.Cq

I. INTRODUCTION

The determination of the properties of strongly interacting matter at high temperatures and baryon densities is one of the main goals of today's high-energy physics. However, not many tools are available for such a difficult task. Due to the fermion sign problem of quantum chromodynamics (QCD) at nonvanishing (real) quark chemical potential, Monte Carlo calculations on the lattice are not feasible in this regime due to the lack of an importance sampling procedure that is free of ambiguities [1,2]. An alternative approach is that of chiral effective models for QCD, which have been successfully utilized for many decades [3,4]. In this work, we shall adopt one such model, the three-flavor Polyakov-quark-meson (PQM) model [5–8]. It has become quite popular in the last years due to its close relationship with the linear sigma model and its agreement with results from lattice calculations of thermodynamical quantities at zero baryon chemical potential.

As discussed for example in Refs. [9–11], not only QCD, but also effective models that possess gauge degrees of freedom, present the sign problem at finite chemical potential μ, even at the mean-field level. In such models, this is manifest in the appearance of an imaginary part of the in-medium effective potential in equilibrium at $\mu \neq 0$. Since the resulting effective potential at finite chemical potential is a complex function of complex variables, special care must be taken with respect to the meaning of a minimization procedure that leads to the state of equilibrium of the system at any given nonzero temperature T and chemical potential μ. Following an approach similar to the one in Ref. [11] [in the context of the Polyakov-loop extended Nambu-Jona Lasinio (PNJL) model], we propose a change of variables, followed by a simple approximation in the PQM model that renders the in-medium effective potential a real function of real variables. As a consequence, the effective potential is, in this approach, a real function that possesses minima, as demanded by general field-theoretical arguments applied to systems in equilibrium.

The implementation of such an approximation scheme (that simply accounts for neglecting the imaginary part of the effective potential) of course leads to differences in the predictions made, for example, with the so-called saddle point approach (see, e.g., Ref. [12]). In this approach, the state of thermodynamical equilibrium is found by first restricting the Polyakov loop variables to real variables. Second, all the extrema of the effective potential (i.e., points in which the derivatives of the effective potential with respect to all order parameters vanish) are determined. At a third step, the state of equilibrium is chosen among the extrema as the one with the lowest value of the effective potential. It often happens that the chosen point is not a minimum, but a saddle point of the effective potential. In fact, in this approach, the effective potential often has no minima, but only saddle points.

In this work, we show how the differences between the two approaches are manifest in the T-μ phase diagram of the model. We also briefly discuss differences and similarities between several parametrizations of the

*bruno.mintz.uerj@gmail.com
†r.stiele@thphys.uni-heidelberg.de
‡rudnei@uerj.br
§schaffner-bielich@uni-heidelberg.de

Polyakov loop potential found in the literature (see, e.g., Refs. [13–15]). The saddle point approach is particularly troublesome for the computation of the surface tension in the region of the phase diagram of the model where a first-order phase transition exists. The computation of the surface tension, and thus of nucleation rates, requires a precise definition and location of the minima of the model. This adds another important aspect to our suggested approach, which is that it consistently allows the evaluation of the surface tension between two phases of the model, which are separated by a first-order phase transition. As discussed for example in Refs. [16–25], the surface tension is a crucial parameter for the dynamics of a first-order phase transition in many scenarios of high-energy physics. Roughly speaking, if the surface tension between the stable and the metastable phases in a given phase transition is too high, the phase conversion may be exceedingly slow. In practical terms, a high surface tension can dynamically suppress a first-order phase transition that would be otherwise allowed if only the bulk equilibrium thermodynamics were considered. For this reason, the evaluation of the surface tension from effective models of QCD is a relevant question about strongly interacting systems that can undergo a first-order phase transition, such as the ones produced in relativistic heavy-ion collisions at RHIC, NICA and FAIR, and also in the interior of compact stars. This evaluation, however, is not available from first-principles QCD but can be performed in a relatively straightforward manner using an effective model for QCD (with or without Polyakov loop degrees of freedom), such as the two-flavor quark-meson model [26], the Nambu-Jona Lasinio (NJL) model [27], or the PQM model, which we will be studying in this work. Another goal in this work is to produce a result that at least overestimates the surface tension in the three-flavor PQM model along the line of first-order phase transition in the T-μ plane. This is an interesting result by itself, but it is also an interesting example of a calculation of the surface tension in a theory with multiple order parameters. Notice that the calculation of the surface tension explicitly demands not only the localization of the minima of the effective potential, but also the precise form of the potential between them. We argue that having a real effective potential as a function of real order parameters is crucial for the calculation of the surface tension, as well as for any other quantity in full thermodynamical equilibrium.

The structure of the paper is as follows. After a brief summary of the PQM model, in Sec. II, we will discuss the necessary conditions on the effective potential for the definiteness of thermodynamical equilibrium states and how these apply to the model. We also show how the sign problem explicitly appears in the PQM model at the mean-field level and propose an approximation in order to circumvent it. In Sec. III, for completeness, we start the section by reviewing the general computation of surface tensions in a first-order phase transition. After that, we discuss how to obtain an overestimate of the surface tension of a phase interface in the PQM model. In Sec. IV we show our results for the phase diagram for the PQM model and the surface tension. The implications of these results are also discussed. Finally, in Sec. V, we give our conclusions and final discussions of the obtained results.

II. THE POLYAKOV-QUARK-MESON MODEL AT FINITE T AND μ

In order to incorporate aspects from the physics of chiral symmetry breaking and restoration, as well as from the confinement-deconfinement phase transitions, we adopt an effective model that captures these main features of quantum chromodynamics. In the last years, two such models have gained much popularity, the PNJL model [12,14,28,29] and the Polyakov-loop-extended quark-meson (PQM) model [5–8]. These models may be considered as extensions of the well-known Nambu-Jona Lasinio model [30–32] and the linear sigma model [19,33–37], which provide an effective realization of the chiral symmetry breaking pattern. The physics of confinement is expected to be taken into account by coupling the quark and the meson degrees of freedom with the expectation value of the Polyakov loop.

In this work, our choice will be a PQM model with $2 + 1$ quark flavors, as in Refs. [6,8].

A. The Polyakov loop

Before discussing the model, we briefly introduce the order parameter for (de)confinement with which the sign problem enters in Polyakov-loop extended models.

The Polyakov loop operator is a Wilson loop in temporal direction,

$$\mathcal{P} = P \exp\left(i \int_0^\beta dx_0 A_0(x_0) \right), \tag{2.1}$$

where P denotes path ordering, $\beta = 1/T$ is the inverse of the temperature and A_0 is the temporal component of the gauge field A_μ [38]. With a gauge that ensures the time independence of A_0, we can perform the integration trivially and the path ordering becomes irrelevant [39,40], so that $\mathcal{P} = \exp(i\beta A_0)$. In this form, it is trivial to see that the Polyakov loop variable,

$$\Phi = \frac{1}{N_c} \mathrm{tr}\mathcal{P}, \tag{2.2}$$

is a complex scalar field $\Phi = \alpha + i\beta$. Furthermore, we can rotate the gauge field in the cartan subalgebra $A_0^c = A_0^{(3)}\lambda_3 + A_0^{(8)}\lambda_8$ [41]. Within this diagonal representation, we see that the adjoint Polyakov loop variable becomes simply $\bar{\Phi} = \alpha - i\beta$.

Under gauge transformations concerning center symmetry, the Polyakov loop operator and its variable

are multiplied with a center element Z, $\Phi \to Z\Phi$. In pure $SU(3)$ gauge theory, that can be considered as QCD with infinitely heavy quark masses, the confining phase is center-symmetric and, therefore, $\langle\Phi\rangle = 0$, while deconfinement is characterized by a finite value of the Polyakov loop expectation value, since center symmetry gets broken spontaneously [38]. Real QCD with physical quark masses adds an explicit symmetry breaking term.

B. Formulation of the model

Let us briefly recall a few aspects of the PQM model. The interested reader may refer to e.g., Refs. [6,8,34,37] for more details.

The starting point for our analysis of the equilibrium states of the system is the in-medium effective potential of the theory[1] as a function of the relevant order parameters and thermodynamical control parameters. This effective potential is derived within a mean-field approximation to a theory with constituent quarks minimally coupled to gauge fields and coupled to mesons via a Yukawa-type term. In the leading in-medium contribution from the fermions, the coupling to the color fields effectively becomes a coupling to the Polyakov loop field. The coupling with the mesons is translated into the masses of the quarks via spontaneous and explicit chiral symmetry breaking terms in the self-interaction Lagrangian density for the mesons. The self-interaction in the gauge sector is modeled by a potential energy for the Polyakov loop variable.

In the chiral sector of the theory, the natural choice of order parameters for the $N_f = 2 + 1$ pattern of chiral symmetry breaking are the nonstrange (σ_x) and strange (σ_y) chiral condensates [37]. In the Polyakov-loop sector, the natural variables are the Polyakov loop itself, Φ, and its conjugate, $\bar{\Phi}$. With these choices, the effective potential is given by the sum of three terms,

$$\Omega = U(\sigma_x, \sigma_y) + \mathcal{U}(\Phi, \bar{\Phi}) + \Omega_{q\bar{q}}(\sigma_x, \sigma_y, \Phi, \bar{\Phi}), \quad (2.3)$$

where the dependence on the thermodynamical control parameters (in this case the temperature T and the quark chemical potential μ) is implicit in the last two terms of Eq. (2.3). Below, we describe in detail each of the contributions appearing in the thermodynamical potential Eq. (2.3).

The first term of the thermodynamical potential (2.3) is the tree-level contribution from the mesonic degrees of freedom and reads

$$U(\sigma_x, \sigma_y) = \frac{m^2}{2}(\sigma_x^2 + \sigma_y^2) + \frac{\lambda_1}{2}\sigma_x^2\sigma_y^2 + \frac{1}{8}(2\lambda_1 + \lambda_2)\sigma_x^4 + \frac{1}{8}(2\lambda_1 + 2\lambda_2)\sigma_y^4 - \frac{c}{2\sqrt{2}}\sigma_x^2\sigma_y - h_x\sigma_x - h_y\sigma_y. \quad (2.4)$$

Since we are studying isospin symmetric matter, we do not distinguish the up and down quark sectors. The mesonic sector has six parameters, that are the mass and couplings m^2, λ_1, λ_2 and c and the explicit chiral symmetry breaking terms, h_x and h_y. They are adjusted to the pion and kaon decay constants f_π and f_K and meson masses of the scalar and pseudoscalar octet, m_π, m_K, $m_\eta^2 + m_{\eta'}^2$ and m_σ. The mass of the sigma meson is still a poorly known number, but the most recent compilation of the Particle Data Group [42] considers that m_σ can vary between 400 and 550 MeV. Once given this set of masses and decay constants, the model parameters are defined. For their explicit expressions, please refer to Refs. [34,37]. The values of the constants we use to calculate these parameters are listed in Table I. We will be using frequently the value $m_\sigma = 500$ MeV for the sigma mass.

The second term in Eq. (2.3) is responsible for including the physics of color confinement through the introduction of a potential energy for the expectation value of the Polyakov loop. The explicit functional form of the potential energy density for the Polyakov loop is still not known directly from first-principle calculations. Instead, a common approach is to choose a functional form for the potential that reproduces crucial features of pure gauge theory and then adjust a set of free parameters to the results for the Polyakov loop and the thermodynamical observables of Monte Carlo lattice calculations. A possible parametrization of the Polyakov loop potential is the polynomial parametrization [5,14],

$$\frac{\mathcal{U}_{\rm poly}(\Phi, \bar{\Phi})}{T^4} = -\frac{b_2(T)}{2}\bar{\Phi}\Phi - \frac{b_3}{6}(\Phi^3 + \bar{\Phi}^3) + \frac{b_4}{4}(\bar{\Phi}\Phi)^2, \quad (2.5)$$

with the temperature-dependent coefficient b_2 defined as

$$b_2(T) = a_0 + a_1\left(\frac{T_0}{T}\right) + a_2\left(\frac{T_0}{T}\right)^2 + a_3\left(\frac{T_0}{T}\right)^3. \quad (2.6)$$

TABLE I. Values of constants to which the parameters of the mesonic potential are adjusted, according to Ref. [42] and value of the *constituent* quark mass of the light (up and down) quarks that we use to fix the quark meson Yukawa coupling in Eq. (2.10).

Constant	f_π	f_K	m_π	m_K	m_η	$m_{\eta'}$	m_σ	m_l
Value [MeV]	92	110	138	495	548	958	400–550	300

[1] As long as we are interested in states of thermal equilibrium of the system, which are described by homogeneous field configurations, the in-medium effective action is reduced to an in-medium effective potential. In the next section, where we study nonhomogeneous states, we will have to consider the effective action instead.

An equivalent polynomial parametrization had been previously proposed in Ref. [13], with different definitions for the coefficients in Eq. (2.5). A simple calculation allows the translation from one set of coefficients to the other. As far as the polynomial parametrization is concerned, we shall stick to the form (2.5).

Another possible parametrization for the effective potential of the Polyakov loop is provided by [15],

$$\frac{\mathcal{U}_{\log}(\Phi,\bar{\Phi})}{T^4} = -\frac{1}{2}A(T)\bar{\Phi}\Phi + B(T) \times \ln[1-6(\bar{\Phi}\Phi)+4(\Phi^3+\bar{\Phi}^3)-3(\bar{\Phi}\Phi)^2], \tag{2.7}$$

where both coefficients are temperature dependent,

$$A(T) = A_0 + A_1\left(\frac{T_0}{T}\right) + A_2\left(\frac{T_0}{T}\right)^2, \tag{2.8a}$$

$$B(T) = B_3\left(\frac{T_0}{T}\right)^3. \tag{2.8b}$$

The form (2.7) of the Polyakov loop potential is called the logarithmic parametrization. In Refs. [13–15] the parameters of both the polynomial and of the logarithmic parametrizations (see next) were adjusted to the lattice simulation of Ref. [43]. They are listed in Table II.

Originally, the parameter T_0 was devised to correspond to the transition temperature in pure Yang-Mills theory $T_0 = 270$ MeV. However, in full dynamical QCD, fermionic contributions and the matter backreaction modify the pure gauge potential to an effective glue potential. Reference [5] estimated this running coupling of QCD by consistency with hard thermal loop perturbation theory calculations [44,45]. They mapped this effect to an N_f-dependent modification of the expansion coefficients of the Polyakov loop potential that results in a N_f-dependence of T_0. The actual value of T_0 for $2+1$ quark flavors with a current strange quark mass of 95 MeV [42] is $T_0 = 182$ MeV.

The authors in Ref. [5] also estimated the dependence of the glue potential with the quark density and mapped it to a quark chemical potential dependence of T_0. Such a dependence can be expected in view of a μ-dependent color screening effect due to quarks. The μ dependence of T_0 suggested in Ref. [5] is implemented as a small correction to the running coupling. Here, we will simply take a more simplistic approach, but without loss of generality, and consider T_0 as a constant parameter.

TABLE II. Parameters of the gauge potential parametrizations for fits to the lattice simulation [43].

Poly	a_0	a_1	a_2	a_3	b_3	b_4
[13]	1.53	0.96	−2.3	−2.85	13.34	14.88
[14]	6.75	−1.95	2.625	−7.44	0.75	7.5
log	A_0	A_1	A_2	B_3		
[15]	3.51	−2.47	15.2	−1.75		

An improved mapping between the pure Yang-Mills potential and the quark-improved glue effective potential in full QCD is discussed and applied in Refs. [46,47] and will be taken into account in a future work.

Finally, the last term of Eq. (2.3) represents the constituent quark sector coupled to the gauge field (represented by the Polyakov loop variables) and to the mesons,

$$\begin{aligned}\Omega_{q\bar{q}}(\sigma_x,\sigma_y,\Phi,\bar{\Phi}) &= -2T\sum_{f=u,d,s}\int\frac{d^3p}{(2\pi)^3}\times\{\ln[1+3(\Phi+\bar{\Phi}e^{-(E_{q,f}-\mu_f)/T}) \\ &\times e^{-(E_{q,f}-\mu_f)/T}+e^{-3(E_{q,f}-\mu_f)/T}] \\ &+\ln[1+3(\bar{\Phi}+\Phi e^{-(E_{q,f}+\mu_f)/T}) \\ &\times e^{-(E_{q,f}+\mu_f)/T}+e^{-3(E_{q,f}+\mu_f)/T}]\},\end{aligned} \tag{2.9}$$

where μ_f is the quark chemical potential for each of the quark flavors.

The constituent light and strange quark masses are, respectively,

$$m_l = \frac{g}{2}\sigma_x \quad \text{and} \quad m_s = \frac{g}{\sqrt{2}}\sigma_y. \tag{2.10}$$

To fix the Yukawa coupling, we choose the constituent quark mass of the light (up and down) quarks to be $m_l = 300$ MeV in the vacuum, where $\langle\sigma_x\rangle = f_\pi$. This results in $m_s \simeq 417$ MeV for the constituent strange quarks.

Notice that the dependence of $\Omega_{q\bar{q}}$ with the chiral condensates σ_x and σ_y in Eq. (2.9) is implicit in the quasiparticle dispersion relation for the constituent quarks,

$$E_{q,f} = \sqrt{k^2+m_f^2}. \tag{2.11}$$

One last comment should be made about the vacuum (or sea) terms of the in-medium effective potential. Many comparative studies within the NJL and linear sigma models and comparisons with functional calculations [7,48,49] have shown that vacuum terms can change qualitatively the structure of the T-μ phase diagram. In particular, if the sigma meson mass is sufficiently large, the line of first-order phase transition can eventually disappear due to the effect of the fermionic vacuum contribution at one loop [36,50,51]. In the present work, although we neglect the vacuum terms from both fermionic and bosonic fields, we adopt mainly a low value of the sigma mass, $m_\sigma = 500$ MeV. Such a low value has been shown to allow for a first-order transition at low temperatures even with the inclusion of fermionic vacuum contributions only (see for instance Ref. [8] and references therein). Therefore, we believe that the no-sea approximation does not spoil the general conclusions of this work. Still, we agree with the authors of Ref. [51] that all the contributions from all fields

of a model should be consistently taken into account, that is the case in functional calculations [48,49]. In this direction, a full study of the renormalized one-loop contributions from quarks and mesons in the PQM model will be taken into account in a future work [52].

C. Thermodynamical equilibrium

Given the temperature T and the quark chemical potential μ, the effective potential (2.3) is then given as a function of the four order parameters of the model, σ_x, σ_y, Φ and $\bar{\Phi}$. In thermal equilibrium, the field configurations that contribute the most to the partition function are those that minimize the in-medium effective potential (or the in-medium effective action, for nonhomogeneous systems). All other extrema of the effective action are exponentially suppressed and give negligible contributions to the equilibrium thermodynamics of the system.

Even though this issue has already been addressed before in the literature (e.g., in Refs. [9,11]), we believe that it should be discussed more thoroughly, especially in the context of the PQM model. Our main motivations for pressing on this point are (1) theoretical consistency, (2) the fact that the results from the two approaches (the saddle point approach and the present one) are different, and (3) that only with equilibrium states described by minima of the effective potential can one calculate quasiequilibrium properties of the system, such as the surface tension in a first-order phase transition, as we already commented above in Sec. I.

The one-loop effective potential of the PQM model at finite temperature and quark chemical potential, as defined in Eq. (2.3), is a complex function of complex variables. Therefore, it can have no minima and, as it stands, it cannot provide a standard description for a thermodynamical system in equilibrium. Finally, it makes sense to identify the extrema of a function with maxima, minima and saddle points only if it is a real function of real variables.

In order to make this statement clearer, let us explicitly identify the real and imaginary parts of the effective potential at finite T and μ.[2] Thus, we must write down the effective potential in terms of these real variables only.

Let us start by making a change of variables in the potential by introducing the real and imaginary parts of the Polyakov loop variables as

$$\alpha \equiv \frac{\Phi + \bar{\Phi}}{2} \quad \text{and} \quad \beta \equiv \frac{\Phi - \bar{\Phi}}{2i}. \tag{2.12}$$

The polynomial potential (2.5) and the logarithmic potential (2.7), respectively, can be both rewritten as functions of the real variables α and β as

$$\frac{\overline{\mathcal{U}}_{\text{poly}}(\alpha,\beta)}{T^4} = -\frac{b_2}{2}(\alpha^2+\beta^2) - \frac{b_3}{3}(\alpha^3 - 3\alpha\beta^2) + \frac{b_4}{4}(\alpha^2+\beta^2)^2 \tag{2.13}$$

and

$$\frac{\overline{\mathcal{U}}_{\log}(\alpha,\beta)}{T^4} = -\frac{A(T)}{2}(\alpha^2+\beta^2) + B(T)\log[1 - 6(\alpha^2+\beta^2) + 8(\alpha^3 - 3\alpha\beta^2) - 3(\alpha^2+\beta^2)^2]. \tag{2.14}$$

We now turn to the contribution from the quarks at finite temperature and chemical potential. Once Φ and $\bar{\Phi}$ are complex-valued variables, the potential (2.9) can take complex values. Let us rewrite it as a function of real variables to make this statement explicit.

Dropping the flavor indexes to keep the notation simpler, we define

$$z_+ \equiv 1 + 3(\Phi + \bar{\Phi}e^{-(E-\mu)/T})e^{-(E-\mu)/T} + e^{-3(E-\mu)/T} \tag{2.15}$$

and

$$z_- \equiv 1 + 3(\bar{\Phi} + \Phi e^{-(E+\mu)/T})e^{-(E+\mu)/T} + e^{-3(E+\mu)/T}, \tag{2.16}$$

such that (2.9) can now be written as

$$\Omega_{q\bar{q}} = -2T\sum_f \int \frac{d^3p}{(2\pi)^3} \log[z_+ z_-]. \tag{2.17}$$

After using (2.12) and performing some straightforward manipulations, one can see that the argument of the logarithm in (2.17) is complex, that is,

$$z_+ z_- = R + iI, \tag{2.18}$$

where

$$\begin{aligned} R \equiv{}& 1 + e^{-3(E-\mu)/T} + e^{-3(E+\mu)/T} + e^{-6E/T} \\ &+ 6\alpha e^{-E/T}\left[\cosh\left(\frac{\mu}{T}\right) + e^{-E/T}\cosh\left(\frac{2\mu}{T}\right)\right] \\ &+ 6\alpha e^{-4E/T}\left[\cosh\left(\frac{2\mu}{T}\right) + e^{-E/T}\cosh\left(\frac{\mu}{T}\right)\right] \\ &+ 9(\alpha^2+\beta^2)(1+e^{-2E/T})e^{-2E/T} \\ &+ 18(\alpha^2-\beta^2)e^{-3E/T}\cosh\left(\frac{\mu}{T}\right) \end{aligned} \tag{2.19}$$

and

$$\begin{aligned} I \equiv{}& 6\beta e^{-E/T}\left[\sinh\left(\frac{\mu}{T}\right) - e^{-E/T}\sinh\left(\frac{2\mu}{T}\right)\right] \\ &+ 6\beta e^{-4E/T}\left[e^{-E/T}\sinh\left(\frac{\mu}{T}\right) - \sinh\left(\frac{2\mu}{T}\right)\right] \\ &- 36\alpha\beta\sinh\left(\frac{\mu}{T}\right)e^{-3E/T}. \end{aligned} \tag{2.20}$$

[2]The following discussion will make it clear that at $\mu = 0$, Φ and $\bar{\Phi}$ are identical and real, so that there is no sign problem in that case.

The complex argument of the logarithm can be written in polar form, $R + iI = \rho e^{i\theta}$, with

$$\rho \equiv \sqrt{R^2 + I^2} \quad \text{and} \quad \theta \equiv \arctan\left(\frac{I}{R}\right), \tag{2.21}$$

so that the potential can be cast in a manifestly complex form,

$$\Omega_{q\bar{q}} = \Omega^R_{q\bar{q}} + i\Omega^I_{q\bar{q}}, \tag{2.22}$$

where

$$\Omega^R_{q\bar{q}} \equiv -2T\sum_f \int \frac{d^3p}{(2\pi)^3} \log[\rho] \tag{2.23}$$

and

$$\Omega^I_{q\bar{q}} \equiv -2T\sum_f \int \frac{d^3p}{(2\pi)^3} \theta. \tag{2.24}$$

The imaginary part (2.24) is the manifestation of the fermion sign problem in the context of the PQM model already at the one-loop level. Note that it is very closely related to the sign problem in the PNJL model as well [2,9,10]. An important aspect of Eq. (2.24) is that it vanishes for $\mu = 0$, so that the effective potential becomes real and free of the sign problem. Furthermore, (2.24) is odd in β, while the real part (2.23) is even in β. This means that we must have $\langle\beta\rangle = 0$, i.e., $\langle\Phi\rangle = \langle\bar{\Phi}\rangle$ for $\mu = 0$, which is a well-known result.

D. A comment about the sign problem

In order to make the sign problem explicit in the PQM model, let us write the grand partition function for the model in the mean-field approximation,

$$\mathcal{Z} = \int [D\vec{\Psi}] \exp\left[-\frac{\mathcal{V}}{T}\Omega(\vec{\Psi})\right], \tag{2.25}$$

where $\mathcal{V}$ is the volume of the space and $\vec{\Psi} = (\sigma_x, \sigma_y, \alpha, \beta)$ formally represents the (real) order parameters.

Notice from Eqs. (2.20) and (2.24) that the imaginary part of the quark contribution is odd in β and all the other contributions are even in β. Let us then split the effective potential in a β-odd part (that coincides with $\Omega^I_{q\bar{q}}$) and a β-even part. The functional integral is to be performed for every possible (real) value that β can assume. We can organize the sum such that the contributions for a given β_0 and its negative $-\beta_0$ are assembled. After a few simple manipulations, one finds

$$\begin{aligned}\mathcal{Z} &= \int_{\beta\in\mathrm{IR}} [D\vec{\Psi}] \exp\left[-\frac{\mathcal{V}}{T}(\Omega_{\beta\text{-even}} + i\Omega^I_{q\bar{q}})\right] \\ &= \int [D\vec{\Psi}] \exp\left[-\frac{\mathcal{V}}{T}\Omega_{\beta\text{-even}}\right] \cos\left[-\frac{\mathcal{V}}{T}\Omega^I_{q\bar{q}}\right].\end{aligned} \tag{2.26}$$

The integrand in the expression (2.26) for the partition function is not positive defined, as a sound Boltzmann factor should be. Recall that the integrand of the partition function (the density matrix elements) corresponds to a sort of probability density, which must be non-negative. This is not true for the grand-partition function (2.26), and we conclude that the PQM model has the sign problem at the mean-field level for a finite chemical potential.

If we insist on writing the partition function (2.26) in the same form as (2.25), we end up with

$$\hat{\Omega} = \Omega_{\beta\text{-even}} - \frac{T}{\mathcal{V}} \log\left[\cos\left(\frac{\mathcal{V}}{T}\Omega^I_{q\bar{q}}\right)\right], \tag{2.27}$$

where $\mathcal{V}$ is the volume of space. This function is not physically acceptable as an effective potential. First, it is a volume-dependent effective potential (therefore, it is not intensive), and second, it is not defined in the thermodynamical limit $\mathcal{V} \to \infty$.

One possibility to circumvent the sign problem, as indicated in Ref. [11], is to treat the imaginary part of the effective potential perturbatively in an expansion in powers of $T/\mathcal{V}$. In the first order of the approximation (which the authors of Ref. [11] identify with the mean-field approximation), one simply ignores the imaginary part (2.24) of the effective potential at finite chemical potential.[3] However, if one neglects $\Omega^I_{q\bar{q}}$, the expectation value of β is zero due to the even parity of $\Omega^R_{q\bar{q}}$ with respect to β. As a consequence, the difference $\langle\bar{\Phi} - \Phi\rangle = 0$, which is in disagreement with complex Langevin [53] and Monte Carlo simulations [1,2]. In spite of this setback, we understand that our approach is simply an approximation scheme that has the strong theoretical advantage of dealing with the well-established minimization procedure for finding the state of equilibrium.

E. Finding the minima of the effective potential

From now on, we shall neglect the imaginary part of the effective potential, as explained before, i.e., consider

$$\bar{\Omega} = U(\sigma_x, \sigma_y) + \bar{\mathcal{U}}(\alpha, \beta) + \Omega^R_{q\bar{q}}(\sigma_x, \sigma_y, \alpha, \beta). \tag{2.28}$$

Given the temperature T and the quark chemical potential μ, the effective potential (2.28) is then given as a function of the four order parameters of the model, σ_x, σ_y, α and β. In equilibrium, the expected values for the order parameters are given by minimizing the effective potential (2.28) with respect to each of them. Therefore, the first necessary condition is to find a point in the order parameter space such that

[3]In this model, ignoring $\Omega^I_{q\bar{q}}$ is equivalent to taking the modulus of the Dirac determinant that is tacitly present in (2.26).

$$\frac{\partial\bar{\Omega}}{\partial\sigma_x} = \frac{\partial\bar{\Omega}}{\partial\sigma_y} = \frac{\partial\bar{\Omega}}{\partial\alpha} = \frac{\partial\bar{\Omega}}{\partial\beta} = 0, \tag{2.29}$$

when the derivatives are evaluated at the extrema.

The second condition is the positivity of all the eigenvalues of the 4×4 Hessian matrix

$$\mathcal{H}_{ij} = \frac{\partial^2\bar{\Omega}}{\partial X_i \partial X_j}, \tag{2.30}$$

with ($X_i = \sigma_x$, σ_y, α, β) evaluated at the points where (2.29) is satisfied.

Hence, we must calculate the first and second derivatives of the effective potential $\bar{\Omega}$ with respect to the order parameters in order to find its minima.

Moreover, once we are interested in phase transitions, our algorithm to find the minima considers the possibility of multiple minima. It performs the following basic steps. With a given starting position in the four-dimensional space of order parameters, the algorithm looks for a point with vanishing gradient (2.29). As a second step, the eigenvalues of the Hessian matrix (2.30) are evaluated at this point and their signs are checked: if they are all positive, this point is a minimum and it is saved as such; otherwise, it is either a saddle point or a maximum and, therefore, it is discarded. Next, another starting position in the order parameter space is tried, and the procedure is repeated. If the point found is a minimum, it is compared to the previous points: if all its four coordinates are sufficiently close to any of the other points (within 1%), it is discarded; otherwise, it is saved as a new minimum. By sweeping a sufficiently wide window in the parameter space, this is a simple algorithm able to find all the minima of the effective potential.

The thermodynamical state of equilibrium for each given T and μ is given by the values of the order parameters at the global minimum of the effective potential, found after the prescription described above. This allows us to describe any thermodynamical quantity of equilibrium. Particularly, we can study the behavior of the order parameters as functions of the temperature and chemical potential, as well as the phase diagram of the model. Moreover, finding the minima of the effective potential at the vicinity of a first-order phase transition allows the description of the dynamics of the transition. More specifically, one can calculate the surface tension between the two phases, as we discuss in the next section. Our results will be discussed in Sec. IV.

F. The saddle point approach

In the literature dedicated to the thermodynamics of strongly interacting systems described by chiral models coupled to the Polyakov loop, such as the PNJL and PQM models, the most common method to determine the state of thermodynamical equilibrium is sometimes called the saddle point approach. It consists of finding the points in which the in-medium effective potential of the theory has vanishing derivatives with respect to the order parameters, as in Eq. (2.29). These extrema, however, are not usually required to be minima of the effective potential. Actually, the effective potential often has no minimum whatsoever as a consequence of one of the two following reasons. Either the effective potential is considered in full, so that it is a complex function of complex variables (as we have discussed previously), or the Polyakov loop variables are restricted to being real (instead of complex) numbers (even before their expectation values are evaluated). In the first case, no minimum can be defined because the effective potential is complex valued. In the second case, it can be easily seen that the effective potential is unbounded from below [5].[4]

The approach we propose in this section leads to predictions that differ from those made by the saddle point approach at $\mu \neq 0$. Some of these differences will be briefly discussed later on in Sec. IV.

III. NUCLEATION IN THE PQM MODEL

A. Homogeneous thermal nucleation

The dynamics of a first-order phase transition at small metastability can be described by phenomenological droplet nucleation models [16,54–57]. In such a family of models, the transition between a metastable and a stable phase takes place by the appearance and growth of domains (droplets or bubbles) of the stable phase inside the metastable phase. The phase conversion is finished when these domains grow and coalesce completely. In any case, a minimum-sized bubble is needed for the beginning of the phase transition, as can be inferred from the following heuristic argument. The bulk free energy density of the metastable phase (often called "false vacuum") is, by definition, higher than that of the stable phase (the "true vacuum"). Therefore, the conversion of a given fraction of the system into the stable phase makes the bulk free energy of the whole system lower. However, given that such a conversion takes place within a connected domain of the system (most likely in a spherical bubble [58]), an interface is needed in order to separate the (stable) interior from the (metastable) exterior of this domain. Once the creation of an interface represents an energy cost, the mechanism of phase conversion through bubble nucleation settles a competition between the free energy gain from the phase conversion of the bulk and the energy cost from the creation of an interface. Roughly, one can say that the free energy shift due to the appearance of a spherical bubble of the stable phase of radius R inside a metastable system is

[4]Just consider $\Phi = 0$ in Eq. (2.5) or in Eq. (2.7), and we can realize that the Polyakov loop potential is unbounded from below for $\bar{\Phi} \to \infty$.

$$\Delta F_b = \left[\frac{4\pi}{3}R^3 f_{\text{stable}} + 4\pi R^2 f_{\text{wall}}\right] - \left[\frac{4\pi}{3}R^3 f_{\text{metastable}}\right] = \frac{4\pi}{3}R^3\Delta f + 4\pi R^2 f_{\text{wall}}, \tag{3.1}$$

where f_{stable} and $f_{\text{metastable}}$ are, respectively, the bulk free energy densities of the stable and metastable phases, and f_{wall} is the surface energy density of the bubble wall, that is, the surface tension of the interface between the two phases. This formula clearly shows the competition between bulk (negative) and surface (positive) contributions. Notice that the shift in the bulk free energy ($\Delta f \equiv f_{\text{stable}} - f_{\text{metastable}} < 0$) is proportional to the volume of the bubble, while the surface free energy cost is proportional to its area. For the nucleation of small bubbles, the energy cost is higher than the energy gain. Therefore, small bubbles shrink. On the other hand, a very large bubble represents a large bulk energy gain, which is higher than the surface energy cost in creating the bubble. As a consequence, large bubbles tend to grow even more and to occupy the whole system, completing the phase transition. Consequently, this energy competition implies the existence of a so-called critical bubble: any bubble smaller than the critical bubble will shrink and any larger bubble will grow and drive the phase conversion. For this reason, the critical bubble is the crucial object in the theory of dynamical first-order phase transitions of slightly metastable systems.

The appearance of a bubble (critical or not) of the stable phase inside a metastable system is a natural consequence of the never-ending thermal and quantum fluctuations of any thermodynamical system sufficiently close to a first-order phase transition. As we just discussed, each bubble created by these fluctuations may grow or shrink, depending on its energy budget with regard to a homogeneous metastable phase. One should also have in mind that larger fluctuations (like a critical bubble) should be less common than smaller ones. Although small bubbles are frequently created, they rapidly disappear and do not contribute to the process of phase conversion (with the exception in a weak first-order phase transition, when coalescing subcritical fluctuations [59,60] can complete the phase transition without the nucleation of critical bubbles). Only those that have a size equal to or larger than the critical bubble have a decisive role. The smallest (and therefore the most probable) among them is the critical bubble. This means that the mean time that it takes for random fluctuations to create a critical bubble is the shortest time scale for the creation of a lasting domain of the stable phase, which is the dynamical seed of the phase conversion.

Let us assume that the system is in a metastable state in quasiequilibrium with a reservoir with intensive coordinates generically represented by $\mathcal{R}$ (e.g., temperature, chemical potential, etc). Being metastable, bubbles of the stable phase with different sizes randomly appear and subsequently disappear. This process keeps happening until a critical bubble is nucleated and the phase conversion effectively starts. It can be shown by different approaches that the rate at which critical bubbles are nucleated per unit time, per unit volume can be expressed in the form [16,17,54,61–63]

$$\Gamma(\mathcal{R}) = \mathcal{P}(\mathcal{R})\exp\left[-\frac{\Delta F_b(\mathcal{R})}{T}\right], \tag{3.2}$$

where T is the temperature of the system in equilibrium with the reservoir. The pre-exponential factor (or "prefactor") $\mathcal{P}(\mathcal{R})$ corresponds to the probability for a critical bubblelike field fluctuation ϕ_b to be generated and grow [16–18]. The last factor in (3.2) is a Boltzmann factor in which $\Delta F_b(\mathcal{R})$ is the shift of free energy (as compared to the homogeneous metastable phase) due to the formation of a critical bubble. It can be easily shown that $\Delta F_b(\mathcal{R})$ can be cast as in (3.1) for a small degree of metastability, where the thin-wall approximation is valid [64] and where it is proportional to $f_{\text{wall}}^3/(\Delta f)^2$. In spite of the general importance of the prefactor in (3.2), its specific form is not crucial for the nucleation rate at a small degree of metastability. Close to the coexistence of both phases, it shows a proportionality to $f_{\text{wall}}^{7/2}/\Delta f$, so that the nucleation rate is strongly dominated by the exponential factor [17]. For this reason, it will be enough to focus on the free energy shift in this work.

The process of bubble nucleation in an impurity-free environment is called homogeneous nucleation. In this work we shall only consider the process of homogeneous nucleation, which is not the most common in natural environments, such as in a boiling liquid. In such cases, the presence of impurities can drastically accelerate the nucleation of bubbles, and the process is called inhomogeneous nucleation (which is also the case when subcritical thermal fluctuations can dominate [59,60]). The process of inhomogeneous nucleation can be orders of magnitude faster than homogeneous nucleation because impurities (like dust) often reduce the free energy cost for the formation of a critical bubble, raising the probability for its formation [65,66]. We do not consider it in this work for two reasons. First, we wish to underestimate the nucleation rate and inhomogeneities could only increase this rate, and second, we wish to keep the approach as simple as possible.

B. The coarse-grained free energy for a single scalar order parameter

As discussed in Refs. [18,64,67,68], the nucleation rate of critical bubbles can be calculated from the microphysics using semiclassical methods in Euclidean thermal field theory. We stress the importance of considering the effective action in the problem of bubble nucleation, and not simply the effective potential, once a critical bubble is clearly a nonhomogeneous field configuration. For simplicity, let us start with the Euclidean Lagrangian density

for a single scalar order parameter field (which we generically call ϕ) of the form,

$$\mathcal{L}_E = \frac{1}{2}(\partial_\mu \phi)^2 + V(\phi). \tag{3.3}$$

In this simple model, one assumes that the order parameter for a system in thermodynamical equilibrium is given by the expectation value of ϕ. In general, it depends on the properties of the reservoir, such as its temperature or chemical potential, which we generally denote by $\mathcal{R}$. The (Euclidean) action is

$$S_E[\phi, \mathcal{R}] = \int_0^\beta d\tau \int d^3x \mathcal{L}_E[\phi(\mathbf{x}, \tau)]. \tag{3.4}$$

In the high-temperature limit, $\beta \equiv 1/T \to 0$, the imaginary time dependence of the order parameter can be neglected [67] and, therefore, we make the approximation

$$S_E[\phi, \mathcal{R}] \equiv \frac{F[\phi, \mathcal{R}]}{T}, \tag{3.5}$$

where one identifies

$$F[\phi, \mathcal{R}] = \int d^3x \left[\frac{1}{2}(\nabla\phi)^2 + V_{\rm eff}(\phi, \mathcal{R})\right], \tag{3.6}$$

with the coarse-grained free energy of the system. Notice that the coarse-grained free energy is a sort of dimensionally reduced effective action, so that the tree-level potential $V(\phi)$ must be replaced by the medium-dependent effective potential $V_{\rm eff}(\phi, \mathcal{R})$. In full thermodynamical equilibrium, the minimization of the coarse-grained free energy (which is equivalent to the minimization of the Euclidean action) is achieved by a constant field configuration $\phi(\mathbf{x}) = \phi_0$ so that the gradient term vanishes, and $V_{\rm eff}(\phi_0, \mathcal{R})$ must be a global minimum of $V_{\rm eff}$.

The possibility of a metastable state arises when $V_{\rm eff}$ develops some local minimum other than the global minimum at $\phi = \phi_0$. In this framework, a metastable state is described by a constant field configuration ϕ_f that is a local minimum of $V_{\rm eff}$. For this reason, this second minimum is often called a false vacuum of the potential, while the global minimum is called the true vacuum of the theory, $\phi_t \equiv \phi_0$. A bubble is then represented as a nonhomogeneous, spherically symmetric field configuration $\phi(r)$, such that [19,20,64]

$$\lim_{r\to\infty} \phi(r) = \phi_f \quad \text{and} \quad \frac{d\phi}{dr}(0) = 0, \tag{3.7}$$

where ϕ_f is the value of the order parameter field at the false vacuum. That is, away from the center of the bubble, the system is in the metastable phase. But, in the vicinity of its center, the field configuration should be close to the stable minimum (but not necessarily exactly on it).

The critical bubble is a saddle point field configuration ϕ_b that extremizes the functional F, i.e., it solves the Euler-Lagrange equation,

$$\frac{\delta F[\phi; T]}{\delta \phi(\mathbf{x})} = 0 \Rightarrow \nabla^2\phi(\mathbf{x}) - \frac{\partial V_{\rm eff}}{\partial \phi}[\phi(\mathbf{x})] = 0. \tag{3.8}$$

It can be shown [58] for a wide class of Lagrangians, including (3.3), that the smallest value of F indeed corresponds to a spherically symmetric solution of (3.8), $\phi(r)$, so that the equation to be solved is now the nonlinear ordinary differential equation,

$$\frac{d^2\phi(r)}{dr^2} + \frac{2}{r}\frac{d\phi(r)}{dr} = \frac{\partial V_{\rm eff}}{\partial \phi}[\phi(r)], \tag{3.9}$$

with the boundary conditions (3.7).

The coarse-grained free energy associated with a spherical bubble ϕ_b is then

$$F_b = 4\pi \int_0^\infty dr r^2 \left\{\frac{1}{2}\left[\frac{d\phi_b(r)}{dr}\right]^2 + V_{\rm eff}[\phi_b(r)]\right\}, \tag{3.10}$$

which directly follows from (3.6).

Once the solution for (3.9) and (3.7) is found, that is, the critical bubble profile $\phi_{\rm crit}(r)$, the shift in the coarse-grained free energy due to the appearance of a critical bubble,

$$\Delta F_b(\mathcal{R}) = F[\phi_{\rm crit}; \mathcal{R}] - F[\phi_f; \mathcal{R}], \tag{3.11}$$

needed in the nucleation rate (3.2), can be readily calculated.

For a generic effective potential $V_{\rm eff}$, the solution of (3.9) with boundary conditions (3.7) cannot be obtained analytically. However, an approximate solution can be found when the system is very close to the coexistence line, so that it is slightly metastable and the thin-wall approximation [61,64,67] is applicable. Within these limits, the coarse-grained free energy shift (3.11) can be well approximated by the expression

$$\Delta F_b(\mathcal{R}) = \frac{16\pi}{3}\frac{\Sigma^3}{(\Delta V_{\rm eff})^2}, \tag{3.12}$$

where

$$\Sigma(T) \equiv \int_0^\infty dr \left[\frac{d\phi_{\rm crit}(r)}{dr}\right]^2 \tag{3.13}$$

is the surface tension of the critical bubble interface between the phases. Notice that the surface tension is calculated directly from the critical bubble solution $\phi_{\rm crit}$. It must be so because the surface tension must contain information about how the system reacts to inhomogeneities (e.g., a wall). That is, any description of a critical bubble has to take into account more than just the bulk thermodynamics. This is the reason why the coarse-grained free energy (3.6) is needed in the formalism for bubble nucleation.

The quantity $\Delta V_{\rm eff} = V_{\rm eff}(\phi_t) - V_{\rm eff}(\phi_f)$ is the difference between the bulk free energy in the two homogeneous vacua. In the grand canonical potential, it can be identified as $\Delta V_{\rm eff}(T, \mu) \equiv -\Delta p(T, \mu)$, i.e., minus the difference of

pressures between the two phases. Using the thin-wall approximation, the surface tension integral (3.13) can be calculated without solving for the profile. After changing variables from r to ϕ, one finds

$$\Sigma(\mathcal{R}) = \int_{\phi_t}^{\phi_f} d\phi \sqrt{2V_{\rm eff}[\phi;\mathcal{R}]}, \tag{3.14}$$

so that only the effective potential $V_{\rm eff}[\phi;\mathcal{R}]$ is needed to calculate $\Sigma(\mathcal{R})$ in the thin-wall approximation. Notice that $V_{\rm eff}$ is normalized so that its global minimum is located at $\phi = \phi_t = 0$. Exactly at the coexistence points, where the thin-wall approximation is exact, the minima are degenerate with $V_{\rm eff} = 0$.

As a last remark, let us notice that the surface tension cannot be correctly defined unless ϕ_t and ϕ_f are actual minima of the effective potential. This a further motivation for the careful approach discussed in the previous Sec. II.

C. The coarse-grained free energy for the Polyakov-quark-meson model

In order to calculate the free energy shift $\Delta F_b(\mathcal{R})$ due to the nucleation of a critical bubble within the PQM model, we first need to define the coarse-grained free energy functional and then identify an order parameter.

Just as in the case of a single order parameter, the coarse-grained free energy of the PQM model has its origin in the in-medium effective action of the theory. In the PQM model, the Lagrangian density of the chiral fields σ_x and σ_y directly leads to a kinetic term of the form $|\nabla\phi|^2$. The kinetic term for the Polyakov loop variable, however, is not determined *a priori*. For simplicity, once we consider the Polyakov loop order parameters α and β as independent, real variables at finite μ, we assume the kinetic term

$$\mathcal{L}_{\rm kin}[\alpha,\beta] = \frac{\kappa^2}{2}(\partial_\mu\alpha)^2 + \frac{\kappa^2}{2}(\partial_\mu\beta)^2, \tag{3.15}$$

which is motivated by the $Z(3)$-line model of Ref. [69].

Effective models cannot do much more than estimate the value of the kinetic parameter κ. From dimensional arguments, it is estimated to be $\kappa^2 = N_c T_0^2/g_s^2$ [13,69]. Assuming $N_c = 3$ and $\alpha_s = g_s^2/4\pi \simeq 0.3$, we find $\kappa \simeq 0.9T_0$, which is of the order of magnitude of the only scale in the pure glue model, the transition temperature T_0. Another consistent approach is to consider as an input the surface tension of the pure gauge $SU(3)$ theory calculated through lattice Monte Carlo simulations [70,71]and in an effective matrix model [72], $\Sigma_{SU(3)} \simeq 0.016T_0^3$. With a given parametrization of the Polyakov loop potential, the parameter κ can be fitted from the value of the surface tension at $T = T_0$, using Eq. (3.14). We adopt this second approach here in order to fix the parameter κ with the implications discussed in Sec. IV.

The coarse-grained free energy for the PQM model can be written as

$$\mathcal{F}[\sigma_x,\sigma_y,\alpha,\beta] = \int d^3x\Big[\frac{1}{2}(\nabla\sigma_x)^2 + \frac{1}{2}(\nabla\sigma_y)^2 + \frac{\kappa^2}{2}(\nabla\alpha)^2 + \frac{\kappa^2}{2}(\nabla\beta)^2 + \bar{\Omega}(\sigma_x,\sigma_y,\alpha,\beta)\Big], \tag{3.16}$$

where $\bar{\Omega}(\sigma_x,\sigma_y,\alpha,\beta)$ is the effective potential defined in Eq. (2.28).

As discussed previously, the critical bubble is a solution of the four coupled Euler-Lagrange equations that arise from the functional (3.16). There is no general procedure to solve this set of coupled equations, even though some ansatz solutions can be eventually tried for very simple effective potentials [73].

There are two possible ways in which we can tackle the problem. The first is, of course, to numerically solve the four equations that follow from the extremization of $\mathcal{F}$ simultaneously. The exact solution will define a path in the four-dimensional space of order parameters. Notice, however, that this path is in general not in the "valley" that connects the two minima, as can be intuitively seen from the inverted potential mechanical analog.

Let us now argue that our approach will lead us to an overestimate of the surface tension or, equivalently, to an underestimate of the nucleation rate. According to Eq. (3.2), the higher the free energy shift of the critical bubble, the lower is the nucleation rate (at least as long as the thin-wall approximation is valid). Now consider that the exact critical bubble solution is found. Consider also a small deviation from it that follows a different path in the order parameter space. Once the true critical bubble is a saddle point solution in a functional space, one expects that the distorted path will have a higher value of ΔF as compared with the true bubble. Hence, we can (artificially) constrain the configuration path to a given arbitrary line that connects the two vacua in the space of order parameters. This path will give us an overestimate of the free energy and, therefore, of the surface tension. The simplest choice is, of course, a straight line that connects both minima.[5] For example, let $\sigma_x^{(1)}$ and $\sigma_x^{(2)}$ be the values of the σ_x order parameter in the two minima of $\bar{\Omega}$ close to the coexistence line. The interpolation

$$\sigma_x = \xi\sigma_x^{(1)} + (1-\xi)\sigma_x^{(2)} \tag{3.17}$$

is such that for $0 \le \xi \le 1$, the value of σ_x varies from one minimum to the other. If the same function ξ is used to parametrize the path followed by the remaining order parameters,

[5]In the whole range of interest in the T-μ plane, we have always found either one or two minima. The case of three or more minima, which we have not encountered, would lead to a much more complicated analysis.

$$\sigma_y = \xi\sigma_y^{(1)} + (1-\xi)\sigma_y^{(2)},$$
$$\alpha = \xi\alpha^{(1)} + (1-\xi)\alpha^{(2)}, \quad (3.18)$$
$$\beta = \xi\beta^{(1)} + (1-\xi)\beta^{(2)},$$

then this path is a straight line in the four-dimensional order parameter space.

It is now natural to define the four-dimensional order parameter for the PQM model as

$$\vec{\Psi} = (\sigma_x, \sigma_y, \kappa\alpha, \kappa\beta). \quad (3.19)$$

It can be easily shown from Eqs. (3.17) and (3.19) that if we write the coarse-grained free energy (3.16) in terms of the field ξ, it assumes the form

$$\tilde{\mathcal{F}}(\xi) = \int d^3x \left[\frac{h^2}{2}(\nabla\xi)^2 + \tilde{\Omega}(\xi)\right], \quad (3.20)$$

where

$$h^2 = (\vec{\Psi}_0 - \vec{\Psi}_1)^2$$
$$= (\Delta\sigma_x)^2 + (\Delta\sigma_y)^2 + (\kappa\Delta\alpha)^2 + (\kappa\Delta\beta)^2, \quad (3.21)$$

and $\tilde{\Omega}(\xi)$ is the projection of the effective potential $\bar{\Omega}(\vec{\Psi})$ along the straight line defined by (3.17). Notice that the coarse-grained free energy $\tilde{\mathcal{F}}$ is formally equivalent to the single field coarse-grained free energy (3.6) and we can now consider ξ as a scalar order parameter. As a result, the surface tension in the PQM model can be overestimated by

$$\Sigma(\mathcal{R}) = h\int_0^1 d\xi\sqrt{2\tilde{\Omega}[\xi;\mathcal{R}]}, \quad (3.22)$$

where the domain of integration ranges from one minimum of $\bar{\Omega}$ (and thus of $\tilde{\Omega}$) to the other along a straight line path in the four-dimensional order parameter space.

Notice that a path other than a straight line in the space of order parameters would not lead to a simple coarse-grained free energy with the same form as (3.20). In the general case, even the definition of the surface tension should be reformulated. This problem will be treated in a separate work.

In the following section, we present our results for the equilibrium thermodynamics as well as for the surface tension in the PQM model.

IV. RESULTS AND DISCUSSION

We will now present our original results for the $N_f = 2+1$ PQM model for quantities in strict thermodynamical equilibrium, as well as an overestimate of the surface tension of a hadron-quark interface as described by this model. We use the methods and approximations discussed in the previous sections. Here, we call the polynomial parametrization of Ref. [13] "Poly-I," while that of Ref. [14] is called "Poly-II." The logarithmic parametrization of Ref. [15] is referred to as "Log."

Notice that the imaginary part of the effective potential (2.24) is zero for $\mu = 0$, and our scheme has to be completely equivalent to the saddle point approach in this limit (notice that $\alpha \equiv \Phi$ for $\mu = 0$). Our numerical results show that this is true indeed.

In an explicit crosscheck, we calculated the pseudocritical temperatures for deconfinement and chiral symmetry restoration at $\mu = 0$, with the same parameter set of Ref. [6]. The chiral pseudocritical temperature is defined as the peak in the chiral susceptibility $\chi_x \equiv -\partial\langle\sigma_x\rangle/\partial T$, while the deconfinement pseudocritical temperature takes place at the peak of $\chi_P \equiv \partial\langle\alpha\rangle/\partial T$. We found the same pseudocritical temperatures as those in Ref. [6] for the Poly-I and the logarithmic parametrizations at $\mu = 0$. This shows numerically a consistency between our approach and the saddle-point approximation in the regime where both methods have to lead to the same results.[6] However, we must stress, the two approaches do give different predictions at finite quark chemical potential, as expected. This difference is mainly due to the fact that we are explicitly considering only the real part of the effective potential at finite chemical potential. As we have already discussed in Secs. I and II, this is a necessary condition in order to fulfill the need of defining minima and for their existence in the thermodynamical potential, which can only be achieved through the reality of the effective potential. In the following, we present our original results alongside the corresponding calculations we performed using the saddle point approach for comparison.

Let us first discuss our results for the behavior of the order parameters for the model at $\mu = 0$ for the logarithmic parametrization of the Polyakov loop potential. The behavior for the polynomial parametrizations Poly-I and Poly-II are very similar, and we do not display them here. Our choice of parameters is shown in Table I, with $m_\sigma = 600$ MeV and $T_0 = 270$ MeV. In Fig. 1, we show our results for the expectation value of the chiral condensates σ_x and σ_y (normalized by the vacuum value of the non-strange condensate $\langle\sigma_x\rangle_{\text{vac}} = f_\pi$), as well as for the Polyakov loop variable α. The steep change of the order parameters at around $T = 205$ MeV indicates the pseudocritical temperature of both the chiral and the deconfinement crossovers. (For some other choices of parameters, these pseudocritical temperatures may not coincide [6].)

The low-temperature behavior of $\langle\sigma_x\rangle$ and of $\langle\sigma_y\rangle$ shows little sensitivity to the choice of the Polyakov loop potential, being dominated by the chemical potential-dependent contribution from the mesonic sector.

Next, we observe that at low temperatures, the order parameters have a discontinuity at some finite μ. This signals a first-order phase transition. In Fig. 2 we show

[6]We refer the interested reader to Ref. [6] for the actual values of pseudocritical temperature found within the $N_f = 2+1$ PQM model.

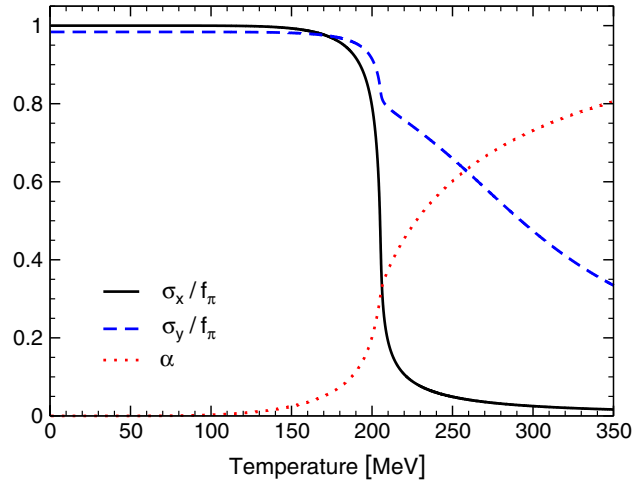

FIG. 1 (color online). Normalized nonstrange condensate ($\langle\sigma_x\rangle/f_\pi$, solid line) and strange condensate ($\langle\sigma_y\rangle/f_\pi$, dashed line) and Polyakov loop variable ($\langle\alpha\rangle$, dotted line) as a function of the temperature for $\mu = 0$. The parameter set used is that of Table I with $m_\sigma = 600$ MeV and $T_0 = 270$ MeV together with the logarithmic Polyakov loop potential.

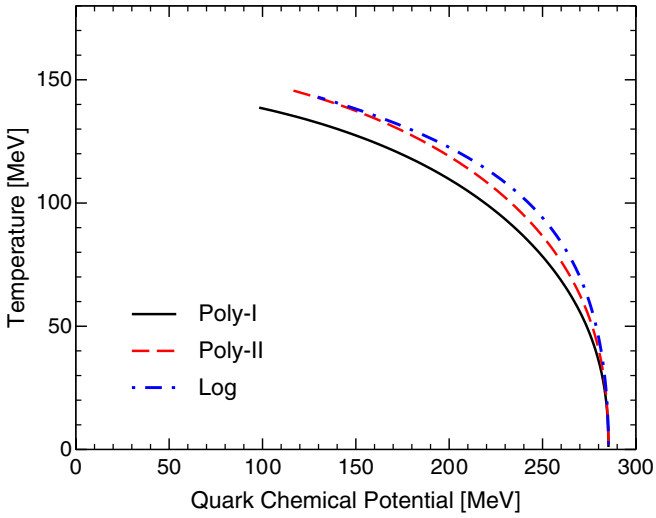

FIG. 3 (color online). Lines of first-order phase transition of the PQM model. The sigma meson mass is $m_\sigma = 500$ MeV and $T_0 = 182$ MeV. Parametrizations of the Polyakov loop potential: Poly-I (full black line), Poly-II (dashed red line) and Log (dash-dotted blue line).

the behavior of the condensates σ_x and σ_y and the Polyakov loop variable α (multiplied by a factor of ten) as a function of the chemical potential for a very low temperature $T = 2$ MeV with sigma mass $m_\sigma = 500$ MeV. Notice that the Polyakov loop variable has a very low expectation value, which grows very slowly at such a low temperature, even at high densities.

Having found a crossover at $\mu = 0$ and a first-order transition at $T = 0$, the next step is to calculate the complete T-μ phase diagram of the model. The phase diagram is shown in Fig. 3 for $m_\sigma = 500$ MeV and $T_0 = 182$ MeV for the three parametrizations of the Polyakov loop potential we have considered in this work.

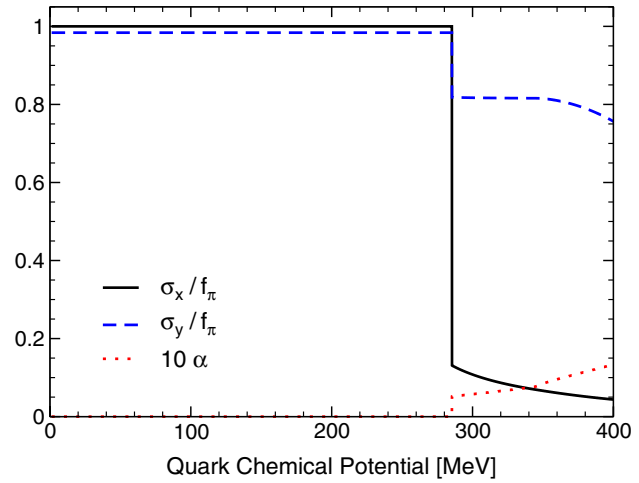

FIG. 2 (color online). Normalized nonstrange condensate ($\langle\sigma_x\rangle/f_\pi$, solid line) and strange condensate ($\langle\sigma_y\rangle/f_\pi$, dashed line) and Polyakov loop variable ($\langle\alpha\rangle$, dotted line) as a function of the chemical potential for $T = 2$ MeV. The parameter set used is that of Table I with $m_\sigma = 500$ MeV and $T_0 = 182$ MeV. For the Polyakov loop potential the logarithmic parametrization is chosen but at this low temperature its influence is negligible.

As mentioned before, the saddle point approach leads to different results to quantities in thermodynamical equilibrium. Comparing the phase diagrams obtained within the two methods, we notice that they are equivalent at $\mu = 0$ (where the sign problem does not exist) and at $T = 0$ (where only the chiral fields are relevant and, again, the sign problem does not exist). For this reason, the phase diagrams can only differ between these two extrema and, in particular, they can lead to different positions for the critical end point (CEP). Table III shows the T-μ coordinates of the CEP found using the method we propose and the saddle-point method. Depending on the parametrization and value

TABLE III. Temperature and quark chemical potential coordinates of the critical end point (CEP) found with the minimization procedure of Sec. II, (T_C, μ_C), and with the saddle point approach, $(T_C, \mu_C)^S$. We choose a sigma meson mass $m_\sigma = 500$ MeV and pure glue transition temperatures $T_0 = 182$ MeV (with effective screening) or $T_0 = 270$ MeV (pure gauge). The parameters not shown in this table are found in Table I.

Parametrization	T_0 [MeV]	(T_C, μ_C) [MeV]	$(T_C, \mu_C)^S$ [MeV]
Log [15]	182	(143, 129)	(143, 128)
	270	(192, 88)	(192, 84)
Poly-I [13]	182	(139, 99)	(140, 92)
	270	(171, 103)	(175, 83)
Poly-II [14]	182	(146, 115)	(152, 80)
	270	(176, 129)	(184, 103)

of T_0 the positions of the CEP found within the two methods can differ significantly. The difference increases with a larger value of the glue transition temperature T_0 and is most pronounced if using the Poly-II parametrization. Due to the slope of the phase transition line around the CEP the differences of the critical chemical potential is larger than that of the temperatures.

The effective potential has always two degenerate minima over the coexistence line of the phase diagram, each one with a different quartet of expected order parameters. In Fig. 4, we show how the coordinates of these minima evolve along the first-order line of the phase diagram, starting from $T = 0$ and finite μ up to the CEP. Notice that the two minima smoothly merge at the CEP with diverging derivative with respect to the temperature. This signals the expected second-order phase transition at the CEP.

The two minima of the potential that are degenerate on the coexistence line persist as a global and a metastable local minimum in some region of the phase diagram around the phase transition line. Going away from the coexistence line, the intervening maximum approaches the local minimum until these two extrema meet and form an inflection point that defines the spinodal line. In Fig. 5 we show the extension of the metastable region of the T-μ phase diagram that is limited by the spinodal lines. The extension is relatively independent of the parametrization of the Polyakov loop potential. We find that the degree of metastability that can be reached is relatively modest.

Let us now study the behavior of the surface tension in the PQM model along the coexistence line for different

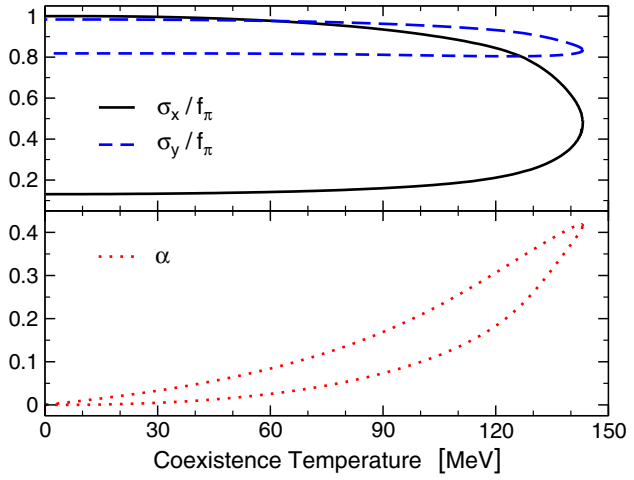

FIG. 4 (color online). Degenerate values of the chiral condensates σ_x and σ_y (upper part) and Polyakov loop variable α (lower part) over the first-order line in the T-μ plane as a function of the coexistence temperature. Notice that the minima merge smoothly at the critical end point. The parameter set used is that of Table I with $m_\sigma = 500$ MeV and $T_0 = 182$ MeV together with the logarithmic parametrization of the Polyakov loop potential.

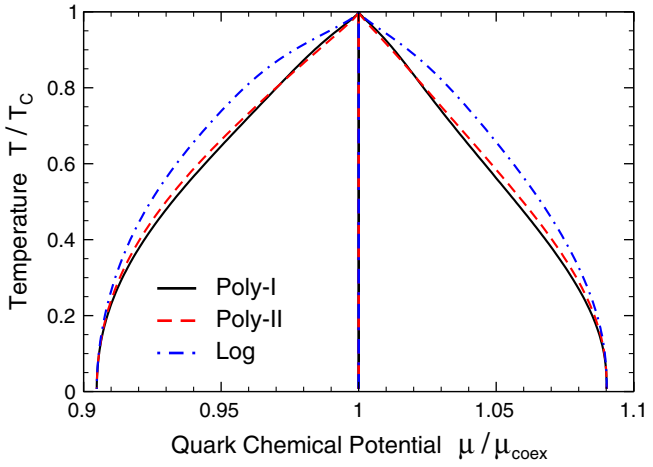

FIG. 5 (color online). Metastable regions of the PQM model for the three considered parametrizations. We compare their extension with respect to the coexistence line ($\mu_{\rm coex}$). The temperature is given relative to the one of the critical end point T_C, see Table III. The sigma meson mass is $m_\sigma = 500$ MeV and $T_0 = 182$ MeV.

parametrizations of the Polyakov loop potential $\mathcal{U}$. The surface tension was evaluated in the thin-wall approximation, according to Eq. (3.14). In Fig. 6, we show the behavior of the surface tension along the first-order transition line for the Poly-I, Poly-II and the Log parametrizations of the Polyakov loop potential. The surface tension for the Poly-II potential is off scale to the other two ones and, therefore, it is shown in the inset of Fig. 6.

Even though equilibrium observables like the behavior of the order parameters and the phase diagram are quite similar for the three parametrizations, there is a remarkable difference between them regarding the surface tension, in particular for the result obtained for the Poly-II parametrization. We interpret this as an artifact of the Poly-II parametrization. Although all parametrizations lead to very similar descriptions of the thermodynamics of the deconfinement transition in equilibrium, they offer different behaviors for the order parameters. At the pure glue transition temperature T_0, the Polyakov loop potentials present two minima, which correspond to the two coexisting values of $\Phi = \bar{\Phi}$ at $T = T_0$. One of these minima is always at $\Phi = 0$, representing the confined phase, while the other sits at some nonzero value $\Phi = \Phi_0$. Using the parameter sets shown in Table II, one can easily see that the Poly-I parametrization possesses the second minimum at $\Phi_0 \simeq 0.6$, while $\Phi_0 \simeq 0.07$ for the Poly-II parametrization and $\Phi_0 \simeq 0.5$ for the Log parametrization. A comparison to the pure gauge $SU(3)$-lattice calculation of Refs. [74,75] shows that one has $\Phi_0^{\rm latt} \simeq 0.4$.

The reason why our results for the surface tension with the Poly-II parametrization are so different can be understood from the definition (3.21). The kinetic parameter κ in (3.15) is fitted from the value of the surface tension in pure

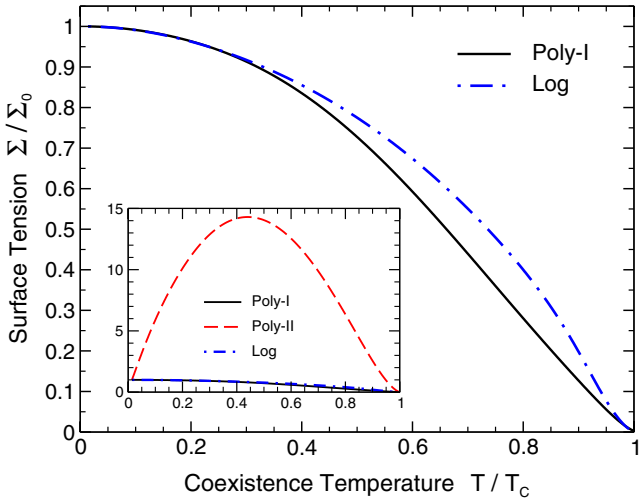

FIG. 6 (color online). Surface tension relative to its zero-temperature value along the first-order transition line in the T-μ phase diagram as a function of the temperature relative to the one of the critical end point. We use the Poly-I and Log parametrizations with $T_0 = 182$ MeV. Inset: The Poly-II parametrization is shown for comparison. The parameter set used is that of Table I with $m_\sigma = 500$ MeV. The other parameters can be found in Tables III and IV.

gauge $SU(3)$-lattice simulations, using Eq. (3.14). After some simple manipulations, one sees that the smaller the barrier between the minima of the pure gauge potential, the larger κ has to be in order to reproduce the known value of $\Sigma_{SU(3)} \simeq 0.016 T_0^3$ [70–72]. Once the Poly-II parametrization leads to a very short and narrow barrier, it gives the large value $\kappa \simeq 160 T_0$. This is two orders of magnitude larger than the values given by the Poly-I and Log parametrizations. As a result, a large value of κ leads to a large coefficient h (3.22) for the Poly-II parametrization and, consequently, to the behavior of the surface tension seen in the inset of Fig. 6. In the following, we only discuss the surface tension derived from the Poly-I and Log parametrizations.

Our results on the zero-temperature surface tension given in Table IV and the temperature dependence of the surface tension seen in Fig. 6 are very similar to those found in Refs. [26,27], which considered the two-flavor QM and NJL models, respectively. This means that the addition of the strange sector does not change appreciably the dynamics of the phase transition at low temperatures and high chemical potentials. Notice that, given a point of phase coexistence in the T-μ plane, $\Delta\sigma_x$ is much larger than $\Delta\sigma_y$, except for conditions very close to the CEP. Therefore, the coefficient h in Eq. (3.22) at low temperatures is barely changed with the contribution from the strange sector. Actually, at low temperatures, the Polyakov loop sector does not give any sensible contribution to the surface tension either. The temperature range in Fig. 6 where the profiles of the surface tension with the Log and Poly-I parametrizations differ indicates where Polyakov loop sector contributes to the surface tension and the difference of the profiles can be considered as an estimate of the uncertainty of the Polyakov loop contribution.

TABLE IV. Low-temperature values of the surface tension at $T = 2$ MeV (in practice, similar to $T = 0$). We choose a sigma meson mass $m_\sigma = 500$ MeV and pure glue transition temperature $T_0 = 182$ MeV. The parameters not shown in this table are found in Table I.

Parametrization	Log [15]	Poly-I [13]	Poly-II [14]
Σ_0 [MeV/fm^2]	13.0	13.0	28.2

A. Implications for proto-neutron stars, the early Universe and heavy ion collisions

The values of surface tension for the $N_f = 2 + 1$ PQM model we found have interesting implications for several physical scenarios. For example, compact stars can be considered as laboratories for nuclear matter at low temperatures and at such high densities that they may contain quark matter [76]. Possible scenarios for the formation of quark matter in compact stars are old accreting neutron stars, proto-neutron stars after a supernova explosion or during the early postbounce evolution of core collapse supernovae [77]. Physical conditions and time scales in these cases imply equilibrium with respect to weak interactions and low electron fractions. Estimates from Ref. [23] show that a hadron-quark phase transition during the bounce phase of a core-collapse supernova can be dynamically suppressed if the surface tension of this phase interface is much larger than, say, 20 MeV/fm^2. The estimates from Refs. [26,27] and this work consistently point towards low values of the surface tension, which would be compatible with the formation of quark matter during the bounce. An observable signal would be a second peak in the neutrino signal dominated by the emission of antineutrinos and with a significant change in the energy of emitted neutrinos [77]. However, none of these calculations really takes into account realistic equations of state for supernova matter, which has to include not only scalar mesons, but also vector mesons, nucleons and, very importantly, leptons. A calculation of surface tension in such a complete model would be most welcome.

In the cosmological case, physical boundary conditions to describe the QCD phase transition in the early Universe include charge neutrality, equilibrium with respect to weak interactions and baryon and lepton asymmetries consistent with observations. Observations of the cosmic microwave background radiation and constraints from primordial nucleosynthesis require a tiny baryon asymmetry at relatively low temperatures ($T \lesssim 1$MeV) [78]. In the standard scenario this observational constraint is extrapolated up to the scale of the QCD phase transition that is then a smooth crossover. In the scenario of little inflation [24], the

Universe enters the QCD era with a very high quark density. As a result, the quark-gluon plasma (QGP) that fills the Universe cools down until it eventually crosses a first-order line of the phase diagram, becoming metastable. While the QGP is metastable, the conditions for a cosmic inflation can be met and the extra quark density becomes very diluted. Observational signals of this evolution include an enhancement of primordial density fluctuations on stellar up to galactic scales, production of galactic and extragalactic magnetic fields and a modification of the gravitational wave spectrum [25,79]. At some point of the expansion, however, the phase transition from a QGP to hadronic matter must happen, most likely through bubble nucleation. In order to be effective, the baryon dilution required by the little inflation scenario needs to be long enough. This requires that the QGP remains metastable even for high degrees of supercooling, something that requires a very low nucleation rate and, therefore, a large value of surface tension. As we have discussed, however, the values of surface tension found with chiral models, including the study we have performed in this work, are relatively small and possibly do not allow the strong metastability required by the scenario of little inflation. However, also a large lepton asymmetry can drive the evolutionary path of the Universe towards larger quark chemical potentials [80].

In heavy ion collisions the phase boundary of hadronic and quark matter is, if at all, crossed twice. First, as formation of a quark gluon plasma in a hadronic gas and then as rehadronization of the fireball. Complications in studying nucleation in heavy ion collisions are the short time scales and the finite size of the system. Additionally, the nucleation rate has to be considered in relation to the expansion time. These conditions can lead to the fact that the system stays in the metastable state close to the spinodal instability and that the dominant mechanism for phase conversion is the alternative scenario to homogenous nucleation, namely spinodal decomposition [19]. Nevertheless, the growth rate of fluctuations by spinodal instabilities is closely related to the surface tension [81,82]. They can lead to observable signatures for the value of the surface tension we found [82]. Additionally, these fluctuations can be amplified by nucleation in the metastable region. The relatively small values of the surface tension we found suggest a early nucleation of small quark-gluon plasma droplets at relatively modest energies like at FAIR's SIS 100 [83]. The details of rehadronization leave their fingerprints on those observables that are sensitive to the life-time of the fireball. Weak supercooling favors the thermal freeze-out to happen in the hadronic phase with impact on particle yields and spectra [84] and a distinct hydrodynamic expansion pattern [19].

V. CONCLUSION

In this work, we have analyzed some thermodynamical properties of the PQM model with $N_f = 2 + 1$ constituent quarks. In particular, we were concerned about the definition of the equilibrium state of a system at temperature T and quark chemical potential μ. As in the case of the PNJL model, the in-medium effective potential of the PQM model is not a real function of real variables and, therefore, it has no minima. As a way to circumvent this problem, we have first rewritten the effective potential in terms of real variables only, such that the real and imaginary parts of the potential are separated. The relation between the imaginary part of the effective potential and the fermion sign problem is discussed. The real effective potential is found to be the appropriate quantity to be minimized and it is a consistent quantity in terms of standard arguments of equilibrium statistical physics. This allowed us to calculate some properties of the model in equilibrium at finite T and μ. In particular, we calculated the evolution of the order parameters as functions of the temperature (for $\mu = 0$) and of the quark chemical potential (for $T = 2$ MeV, which is, in practice, equivalent to $T = 0$). We also calculated the T-μ phase diagram of the model and compared our results to the ones found in the literature using the saddle-point method. The results are equivalent for $\mu = 0$ (where they had to be), but differ for nonzero μ. The phase transition lines of both methods coincide, but the location of the critical end point can be at up to 40% larger chemical potentials using the minimizing method, depending on the Polyakov loop potential parametrization and parameters.

A careful minimization of the effective potential also allowed us to study the problem of homogeneous nucleation of bubbles in a first-order phase transition. More specifically, we calculated the surface tension of an interface between the two phases predicted by the model, a quantity that is crucial for the nucleation rate of bubbles in a first-order phase transition. We saw that the $N_f = 2 + 1$ PQM model yields results very similar to those of the two-flavor NJL and QM models, so that the influence of both the strange quark and the Polyakov loop at low temperatures is small. However, the same cannot be said for higher temperatures, where all contributions become of the same order of magnitude. Our overestimate gives a conservative upper bound of $\Sigma \lesssim 15$ MeV/fm^2 for the surface tension. The actual value, however, may be even lower, not only because of the direct approximations in the calculation of the surface tension, but also due to vacuum terms, which we have neglected and should make the first-order transition weaker at low T and high μ. In any case, this reinforces the trend shown recently in Refs. [26,27] of a low surface tension in chiral models for QCD at finite baryon density. Such a low value would allow a quick hadron-quark phase conversion. This implies interesting implications for several physical scenarios, be it heavy ion collisions, proto-neutron stars or the early Universe.

In summary, the analysis carried out in this work suggests that, in spite of the good agreement of the chiral models at finite T and $\mu = 0$ with lattice calculations, one

should take care when the $\mu \neq 0$ case is addressed. This difficulty is manifest in the nonreality of the equilibrium effective potential for $\mu \neq 0$, even far from any phase transition. Notice that, in principle, the same problem can affect any chiral model with gauge fields coupled to quarks at finite μ, such as the PNJL model. We believe that more consistent solutions to these (and other possible) problems are still needed as they would bring more confidence to further progress in the domain of high chemical potentials of the QCD phase diagram with effective models.

ACKNOWLEDGMENTS

We thank Marcus B. Pinto, Eduardo S. Fraga, Letícia F. Palhares and Jan M. Pawlowski for discussions. The work of B. W. M. and R. O. R. was partially supported by Conselho Nacional de Desenvolvimento Científico e Tecnológico (CNPq). R. O. R. is also partially supported by a research grant from Fundação Carlos Chagas Filho de Amparo à Pesquisa do Estado do Rio de Janeiro (FAPERJ). J. S. B. and R. S. are supported by BMBF under Grants FKZ No. 06HD9127 and 06HD7142, by the German Research Foundation (DFG) within the framework of the excellence initiative through the Heidelberg Graduate School of Fundamental Physics (HGSFP) and through the Helmholtz Graduate School for Heavy-Ion Research (HGS-HIRe) and the Graduate Program for Hadron and Ion Research (GP-HIR) by the Gesellschaft für Schwerionenforschung (GSI), Darmstadt and the Alliance Program of the Helmholtz Association No. HA216/EMMI. R. S. expresses thanks for kind hospitality and support at the Instituto de Física at the Universidade Federal do Rio de Janeiro during part of this project, a research stay that was also supported by the HGS-HIRe abroad program.

[1] P. de Forcrand and O. Philipsen, J. High Energy Phys. 1 (2007) 077.
[2] C. E. Detar and U. M. Heller, Eur. Phys. J. A **41**, 405 (2009).
[3] Y. Nambu and G. Jona-Lasinio, Phys. Rev. **122**, 345 (1961).
[4] M. Gell-Mann and M. Levy, Nuovo Cimento **16**, 705 (1960).
[5] B.-J. Schaefer, J. M. Pawlowski, and J. Wambach, Phys. Rev. D **76**, 074023 (2007).
[6] B.-J. Schaefer, M. Wagner, and J. Wambach, Phys. Rev. D **81**, 074013 (2010).
[7] T. K. Herbst, J. M. Pawlowski, and B.-J. Schaefer, Phys. Lett. B **696**, 58 (2011).
[8] B.-J. Schaefer and M. Wagner, Phys. Rev. D **85**, 034027 (2012).
[9] K. Fukushima and Y. Hidaka, Phys. Rev. D **75**, 036002 (2007).
[10] A. Dumitru, R. D. Pisarski, and D. Zschiesche, Phys. Rev. D **72**, 065008 (2005).
[11] S. Rößner, T. Hell, C. Ratti, and W. Weise, Nucl. Phys. **A814**, 118 (2008).
[12] K. Fukushima, Phys. Lett. B **591**, 277 (2004).
[13] O. Scavenius, A. Dumitru, and J. T. Lenaghan, Phys. Rev. C **66**, 034903 (2002).
[14] C. Ratti, M. A. Thaler, and W. Weise, Phys. Rev. D **73**, 014019 (2006).
[15] S. Rößner, C. Ratti, and W. Weise, Phys. Rev. D **75**, 034007 (2007).
[16] J. S. Langer and L. A. Turski, Phys. Rev. A **8**, 3230 (1973).
[17] L. P. Csernai and J. I. Kapusta, Phys. Rev. D **46**, 1379 (1992).
[18] M. Gleiser, G. C. Marques, and R. O. Ramos, Phys. Rev. D **48**, 1571 (1993).
[19] O. Scavenius, A. Dumitru, E. S. Fraga, J. T. Lenaghan, and A. D. Jackson, Phys. Rev. D **63**, 116003 (2001).
[20] A. Bessa, E. S. Fraga, and B. W. Mintz, Phys. Rev. D **79**, 034012 (2009).
[21] I. Bombaci, P. K. Panda, C. Providência, and I. Vidaña, Phys. Rev. D **77**, 083002 (2008).
[22] I. Bombaci, D. Logoteta, P. K. Panda, C. Providência, and I. Vidaña, Phys. Lett. B **680**, 448 (2009).
[23] B. W. Mintz, E. S. Fraga, G. Pagliara, and J. Schaffner-Bielich, Phys. Rev. D **81**, 123012 (2010).
[24] T. Boeckel and J. Schaffner-Bielich, Phys. Rev. Lett. **105**, 041301 (2010).
[25] T. Boeckel and J. Schaffner-Bielich, Phys. Rev. D **85**, 103506 (2012).
[26] L. F. Palhares and E. S. Fraga, Phys. Rev. D **82**, 125018 (2010).
[27] M. B. Pinto, V. Koch, and J. Randrup, Phys. Rev. C **86**, 025203 (2012).
[28] Á. Mócsy, F. Sannino, and K. Tuominen, Phys. Rev. Lett. **92**, 182302 (2004).
[29] E. Megías, E. R. Arriola, and L. L. Salcedo, Phys. Rev. D **74**, 065005 (2006).
[30] S. Klevansky, Rev. Mod. Phys. **64**, 649 (1992).
[31] M. Buballa, Phys. Rep. **407**, 205 (2005).
[32] P. Costa, M. C. Ruivo, and C. A. de Sousa, Phys. Rev. D **77**, 096001 (2008).
[33] D. Metzger, H. Meyer-Ortmanns, and H. Pirner, Phys. Lett. B **321**, 66 (1994).
[34] J. T. Lenaghan, D. H. Rischke, and J. Schaffner-Bielich, Phys. Rev. D **62**, 085008 (2000).
[35] O. Scavenius, A. Mocsy, I. N. Mishustin, and D. H. Rischke, Phys. Rev. C **64**, 045202 (2001).
[36] E. S. Bowman and J. I. Kapusta, Phys. Rev. C **79**, 015202 (2009).
[37] B.-J. Schaefer and M. Wagner, Phys. Rev. D **79**, 014018 (2009).
[38] A. M. Polyakov, Phys. Lett. **72B**, 477 (1978).
[39] F. Marhauser and J. M. Pawlowski, arXiv:0812.1144.

[40] E. Megías, E. R. Arriola, and L. L. Salcedo, J. High Energy Phys. 1 (2006) 073.
[41] J. Braun, H. Gies, and J. M. Pawlowski, Phys. Lett. B **684**, 262 (2010).
[42] J. Beringer (Particle Data Group), Phys. Rev. D **86**, 010001 (2012).
[43] G. Boyd, J. Engels, F. Karsch, E. Laermann, C. Legeland, M. Lütgemeier, and B. Petersson, Nucl. Phys. **B469**, 419 (1996).
[44] J. Braun and H. Gies, J. High Energy Phys. 6 (2006) 024.
[45] J. Braun and H. Gies, Phys. Lett. B **645**, 53 (2007).
[46] L. M. Haas, R. Stiele, J. Braun, J. M. Pawlowski, and J. Schaffner-Bielich (unpublished).
[47] R. Stiele, L. M. Haas, J. Braun, J. M. Pawlowski, and J. Schaffner-Bielich, Proc. Sci., Confinement X (2013) 215.
[48] J. Braun, L. M. Haas, F. Marhauser, and J. M. Pawlowski, Phys. Rev. Lett. **106**, 022002 (2011).
[49] J. M. Pawlowski, AIP Conf. Proc. **1343**, 75 (2011).
[50] V. Skokov, B. Friman, E. Nakano, K. Redlich, and B.-J. Schaefer, Phys. Rev. D **82**, 034029 (2010).
[51] J. O. Andersen, R. Khan, and L. T. Kyllingstad, arXiv:1102.2779.
[52] B. W. Mintz and R. O. Ramos (unpublished).
[53] F. Karsch and H. W. Wyld, Phys. Rev. Lett. **55**, 2242 (1985).
[54] J. S. Langer, Ann. Phys. (N.Y.) **54**, 258 (1969).
[55] J. D. Gunton, M. S. Miguel, and P. S. Sahni, in *Phase Transitions and Critical Phenomena*, edited by C. Domb and J. L. Lebowitz (Academic Press, London, 1983), Vol. 8.
[56] J. W. Cahn and J. E. Hilliard, J. Chem. Phys. **28**, 258 (1958).
[57] J. W. Cahn and J. E. Hilliard, J. Chem. Phys. **31**, 688 (1959).
[58] S. Coleman, V. Glaser, and A. Martin, Commun. Math. Phys. **58**, 211 (1978).
[59] M. Gleiser and R. O. Ramos, Phys. Lett. B **300**, 271 (1993).
[60] R. O. Ramos, Phys. Rev. D **54**, 4770 (1996).
[61] S. Coleman, Phys. Rev. D **15**, 2929 (1977).
[62] S. Coleman, Phys. Rev. D **16**, 1248 (1977).
[63] C. G. Callan, Jr. and S. Coleman, Phys. Rev. D **16**, 1762 (1977).
[64] S. Coleman, in *Aspects of Symmetry*, edited by S. Coleman (Cambridge University Press, Cambridge, England, 1988), p. 416.
[65] D. Kashchiev, *Nucleation: Basic Theory with Applications* (Butterworth Heinemann, New York, 2000).
[66] H. Vehkamaeki, *Classical Nucleation Theory in Multicomponent Systems* (Springer, New York, 2006).
[67] A. D. Linde, Nucl. Phys. **B216**, 421 (1983).
[68] E. J. Weinberg, Phys. Rev. D **47**, 4614 (1993).
[69] R. D. Pisarski, Phys. Rev. D **62**, 111501 (2000).
[70] B. Beinlich, F. Karsch, and A. Peikert, Phys. Lett. B **390**, 268 (1997).
[71] B. Lucini, M. Teper, and U. Wenger, J. High Energy Phys. 2 (2005) 033.
[72] A. Dumitru, Y. Guo, Y. Hidaka, C. P. K. Altes, and R. D. Pisarski, Phys. Rev. D **86**, 105017 (2012).
[73] R. Rajaraman, *An Introduction to Solitons and Instantons in Quantum Field Theory* (North-Holland, Amsterdam, 1987).
[74] O. Kaczmarek, F. Karsch, P. Petreczky, and F. Zantow, Phys. Lett. B **543**, 41 (2002).
[75] A. Mykkänen, M. Panero, and K. Rummukainen, J. High Energy Phys. 5 (2012) 69.
[76] F. Weber, Prog. Part. Nucl. Phys. **54**, 193 (2005).
[77] I. Sagert, M. Hempel, G. Pagliara, J. Schaffner-Bielich, T. Fischer, A. Mezzacappa, F.-K. Thielemann, and M. Liebendörfer, Phys. Rev. Lett. **102**, 081101 (2009).
[78] D. Boyanovsky, H. J. de Vega, and D. J. Schwarz, Annu. Rev. Nucl. Part. Sci. **56**, 441 (2006).
[79] S. Schettler, T. Boeckel, and J. Schaffner-Bielich, Phys. Rev. D **83**, 064030 (2011).
[80] D. J. Schwarz and M. Stuke, J. Cosmol. Astropart. Phys. 11 (2009) 025.
[81] J. Randrup, Phys. Rev. C **79**, 054911 (2009).
[82] J. Steinheimer and J. Randrup, Phys. Rev. Lett. **109**, 212301 (2012).
[83] J. I. Kapusta, A. P. Vischer, and R. Venugopalan, Phys. Rev. C **51**, 901 (1995).
[84] L. P. Csernai and I. N. Mishustin, Phys. Rev. Lett. **74**, 5005 (1995).